

P.I.V. Flow Characterization Inside a Large-Scale U-Shaped Smooth and Ribbed Rotating Channel

A. Ristori*, I. Da Costa, F. Chedeveigne, P. Roux, D. Carru
 Onera - The French Aerospace Lab, F-91761 Palaiseau, France
 * Corresponding author: arnaud.ristori@onera.fr

Abstract

A research program has been initiated at ONERA with the aim to improve methodology for turbine blade cooling design and tuning by using validated CFD codes. The approach has consisted in designing and manufacturing a specific large-scale U-Shaped rotating cooling channel model in order to set up an experimental database for those types of flows with rotation.

This paper describes the rig and the large-scale U-shaped channel designed and tested in order to set-up an experimental database for non-rotating and rotating flow cases. Experimental results obtained by using the Particle Image Velocimetry (P.I.V.) technique in this new facility named BATHIRE (Test Bench for AeroThermal flows Investigations in a Rotating Environment), as well as associated thermal measurements, are presented. Results agreed well with simulations realized by CEDRE® CFD code developed by ONERA for internal flows.

Nomenclature

D_H	hydraulic diameter (m)
F_{co}	Coriolis force (N)
F_{ce}	centrifugal force (N)
Gr	Grashof number
h	internal heat transfer convection coefficient ($W.m^{-2}.K^{-1}$)
k	thermal conductivity of coolant air flow ($W.m^{-1}.K^{-1}$)
\dot{m}	mass flow rate ($Kg.s^{-1}$)
Nu	Nusselt number, hD_H/k
Nu_0	fully developed, non-rotating Nusselt number from Dittus-Boelter correlation
P	pressure (Pa)
Re	Reynolds number, $\rho \cdot U_{mean} \cdot D_H / \mu$
Ro	Rossby number, $\Omega \cdot D_H / U_{mean}$
T_w	wall temperature (K)
T_{air}	bulk air inlet temperature (K)
U	local radial velocity ($m.s^{-1}$)
U_{mean}	mean bulk flow velocity at the channel inlet ($m.s^{-1}$)
V	local lateral velocity ($m.s^{-1}$)
W	local tangential velocity ($m.s^{-1}$)
X, Y, Z	coordinates in the channel referential
X	coordinate in radial direction (m)
Y	coordinate in lateral direction (m)
Z	coordinate in direction perpendicular to heated wall (m)
μ	viscosity ($kg.m^{-1}.s^{-1}$)
ρ	density ($kg.m^{-3}$)
Ω	rotational speed (rad/s)

1. Introduction

Improvement of modern turbojet performances requires an optimization of turbine blades passages design. Thus, turbine blades' cooling remains a major topic of research interest for turbomachinery industries. Some improvements of aero-engines efficiency and reduction of specific fuel consumption have been achieved thanks to higher combustors efficiency. As a consequence, hot gas temperature is increased and turbine blades' cooling is still a critical design aspect. Turbine blades include internal cooling channels (**Figure 1**) in order to dissipate the thermal energy absorbed by blade walls. Cooling air is extracted from the compressor and injected into the turbine blades; a

portion of this cooling air flow is then ejected through holes or slots at the leading edge and trailing edge of the blade.

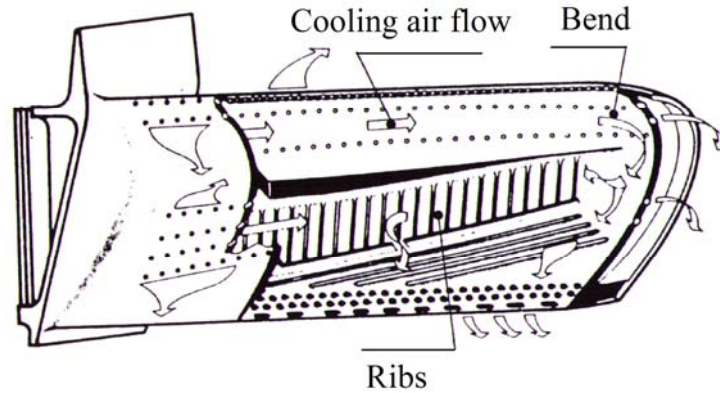


Figure 1: Example of turbine blade internal cavity.

In order to optimize blade cooling, a good understanding of the flow structure inside internal turbulent cooling passages for static and rotating blades is necessary.

Thanks to the availability of more powerful computers and new 3D CFD codes, it is now possible to compute turbulent flow fields inside cooling passages. The development methodology consists in optimizing of cooling through improved design and tuning of the turbine blade passages. Nevertheless, an efficient use of this tool requires the availability of numerical models for heat transfer in internal cooling applications.

Fundamental and applied researches on turbine blade cooling phenomena have been studied experimentally and numerically at ONERA for many years [1-3].

Based upon this background knowledge, ONERA has initiated, in 2006, a new experimental research program [1] with the aim to further improve the methodology for turbine blades passages design and tuning by using validated CFD codes.

The first objective is to validate models and CFD codes [4] in order to generate a reliable numerical tool capable of predicting steady performances of cooling for various configurations (Reynolds and Rossby numbers, centrifugal/centripetal branches, walls heating temperature, ribs geometries, with/without ribs...). The second objective is to provide a better understanding of the aerodynamic and thermal phenomena at play during internal cooling of turbine blades by forced convection.

This paper describes the developed test rig and the large-scale U-shaped channel designed and tested in order to set-up an experimental database for non-rotating and rotating flow cases.

Experimental results obtained by using the Particle Image Velocimetry (P.I.V.) and Infrared thermography techniques in this facility named BATHIRE (Test Bench for AeroThermal flows Investigations in a Rotating Environment) are described. Computational results show that recent models implemented in the CEDRE® CFD ONERA code, are shown to be able to capture the main effects encountered in the aerothermodynamics context of turbine blade cooling systems.

2. Description of experimental facility

The BATHIRE facility [1], which follows another smaller-scale rig named MERCI [2] (rig for studying cooling by internal convection), was specifically designed for the use of modern optical diagnostic tools, such as PIV for measuring the flow velocity fields.

The turbine blade cooling channel model is attached to a support arm (at $X=600$ mm), which contains two passages for air flow inlet and outlet, and rotates in a vertical plane inside an enclosure (non represented in **Figure 2**). The test channel and its support arm are balanced thanks to a counterweight arm located at the opposite diameter. The set is attached to a rotation shaft. This shaft is driven through a belt by a variable-speed electric motor, allowing a maximum rotating speed of 1,000 rpm in clockwise ($\Omega>0$) and counter-clockwise ($\Omega<0$) directions (**Figure 2**).

The test channel (**Figure 3**) is an evolutive section (square and rectangular) U-shaped channel with two branches, where hydraulic diameter is more or less constant and equal to a value within $D_H=50$ mm. For the configuration presented here, the flow enters by the right square section branch of the test model. Dimensions of both test models (branches) are summarized in **Table 1**. At the periphery, both branches are linked through a 180° U-curved bend with a constant height. The test channel design allows the optional installation of ribs on internal walls. The study presented in this paper focuses on the case of smooth and ribbed internal walls in static and rotating conditions.

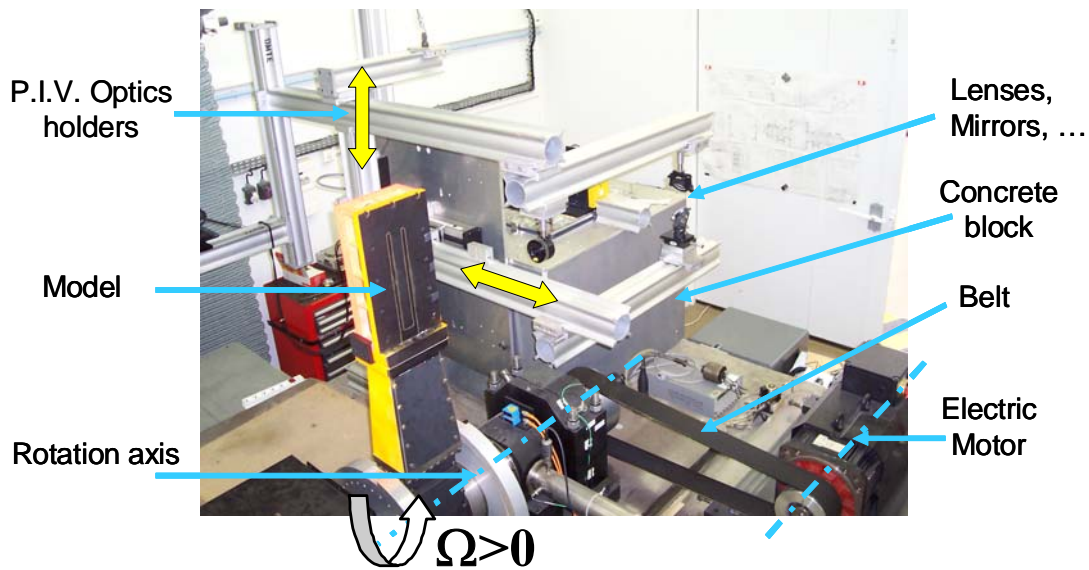


Figure 2: Photograph of the BATHIRE test rig.

The test channel (**Figure 3**) features a large optical access in order to allow optical measurements (PIV, IR thermography...). One sidewall is heated by an electric heater, thus allowing to reach a maximum wall temperature of nearly 350 K, with air flow temperature at 293 K.

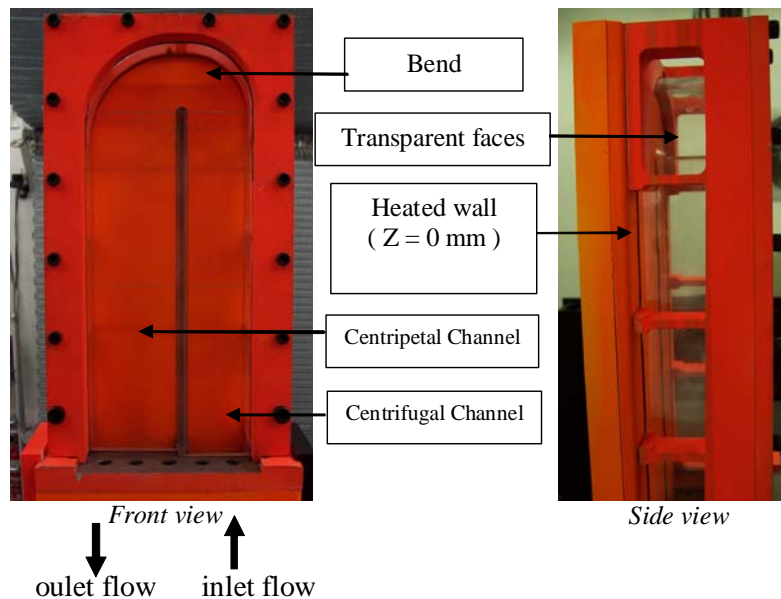


Figure 3: Photographs of the test channel (smooth configuration).

Application of orange fluorescent paint was performed in order to limit the amount of light reflected by stainless steel walls during P.I.V. measurements. Test rig operating range conditions are provided in **Table 2** using the following dimensionless numbers:

- Re =Reynolds number: main flow characteristics.
- Ro = Rossby/Rotation number: Coriolis forces effects.
- Gr =Grashof number: thermal aspect near the heated wall induced by wall to air flow temperature difference.

The values in **Table 2** are comparable to those of real motors.

Table 1: Branches dimensions of the test model.

	Width x Height (mm)	D_H (mm)
Right branch Inlet	50 x 50	50
Right branch Outlet	50 x 44	46.81
Left branch Inlet	70 x 44	54.04
Left branch Outlet	70 x 37	48.41

Table 2: Operating conditions (real engine/BATHIRE rig).

	Re_{DH}	Ro	Gr
Real engine	< 60000	0.045 à 0.1	< $7 \cdot 10^8$
BATHIRE	5000 to 50000	< 3	< $4 \cdot 10^8$

The operating conditions investigated in this paper are the following:

- Reynolds number of 25,000
- Heated stainless steel wall temperature $T_w = 333K$
- Static case: without rotation ($Ro=0$)
- Rotating case: rotation number $Ro=0.33$ corresponding to a rotation speed equal to $\Omega=480$ rpm. Only clockwise direction of rotation ($\Omega>0$) was investigated in this paper.
- Smooth and ribbed channels.

3. PIV arrangement around BATHIRE test rig

In order to characterize the effect of rotation (due to the centrifugal and Coriolis forces) on the flow structure, the mean velocity field inside this channel was investigated.

Figure 4 show the experimental arrangement used for PIV measurements (LaVision® Flowmaster system, Davis®7 data acquisition and processing software). The internal air flow was seeded with olive oil droplets generated by a Laskin nozzle. In order to illuminate droplets, from which Mie-scattering light was observed by a CCD camera, a double-pulse Nd-Yag laser was used (two-cavities Quantel® Laser Twin Model - $\lambda=532$ nm - 120 mJ/pulse). The laser sheets created through a light sheet generator could be moved vertically and horizontally in order to cover the whole test channel volume. This was achieved thanks to a translation stage system which moved simultaneously the laser light sheets and camera.

Particle images were collected through a CCD-12 bits camera (LaVision®) with a frame size of 1280x1024 pixels². Maximum repetition rate of double-frame images is 4 Hz.

Interrogation window size was 16x16 pixels², corresponding to a measurement spatial resolution of 0.96 mm. The cross-correlation function used for data image processing is the standard FFT analysis.

In the channel rotating mode, laser and camera operation were phase-locked with the channel passage thanks to a trigger mechanism. Results presented in this paper were obtained by averaging 150 instantaneous velocity fields and were conducted with Rotation numbers equal to 0 (static case) and 0.33 corresponding to 480 rpm (rotation case) for $Re=25,000$ and $T_w=333$ K for a smooth channel and a ribbed channel.

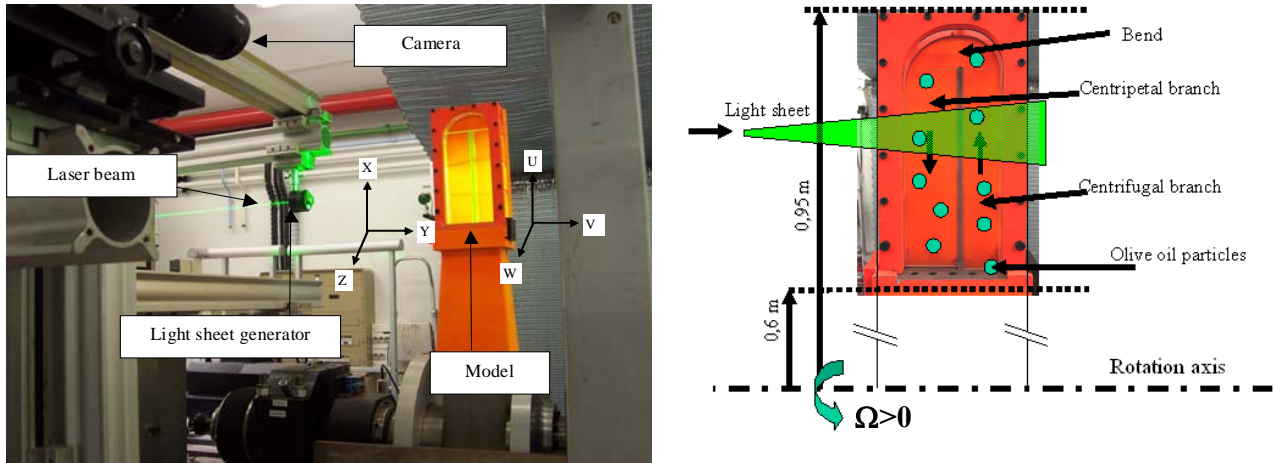


Figure 4: PIV arrangement setup around BATHIRE test rig.

4. Secondary flows characteristics in static and rotating cases

The flow is subjected to centrifugal (F_{ce}) forces and to Coriolis (F_{co}) forces (**Figure 5**) in addition to pressure and friction forces. The Coriolis forces induce secondary flows and distortions of the main flow velocity profiles and consequently modify skin friction and heat transfer coefficients along the walls. The centrifugal forces induce a longitudinal stratification of the pressure. In the static case, the effect of the bend can be detected in the centripetal branch by the presence of two counter-rotating vortices (**Figure 6-a**).

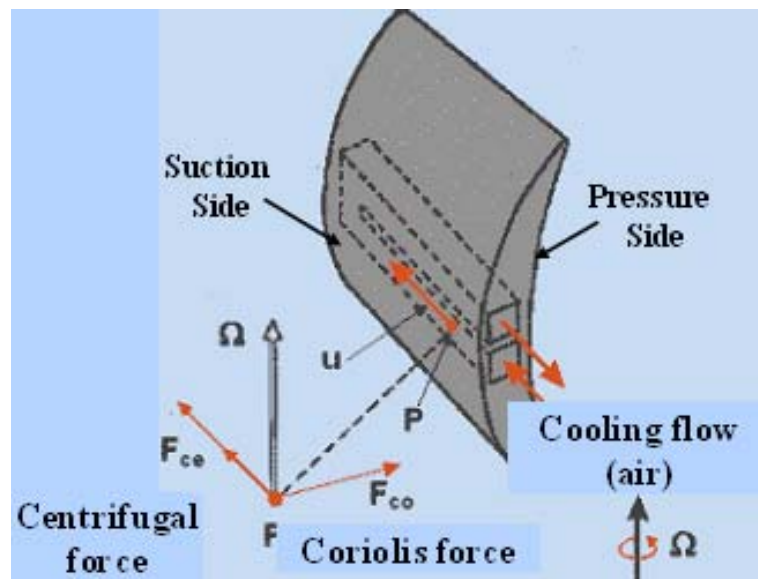


Figure 5 : Centrifugal and Coriolis forces induced by rotation.

In the rotation case, two counter-rotating vortices, which are shifted by 90° compared to the two counter-rotating vortices generated by the bend, are also created in the centrifugal and in the centripetal channel.

The changes of Coriolis forces (F_{co}) direction between centrifugal and centripetal channels opposite swirling motion orientation the results inside the branches (**Figure 6-b**).

The combined effects of bend and rotation observed in the centripetal branch (**Figure 6-c**) are resulting in the creation of one single vortex [2-4].

Those secondary flow motions have a very significant impact on heat transfer coefficients.

Experimental and numerical results show [3] that a rise of the speed of rotation (resulting in an increase of Rotation or Rossby number) leads to a local increase of the internal convective heat transfer coefficient on the pressure side and a decrease on the suction side of the centrifugal branch.

Regarding the centripetal branch, the effect of the bend is almost as significant as the effect of rotation, thus resulting in a single homogeneous vortex. As a consequence, less convective heat transfer coefficients differences exist between the pressure and the suction sides compared to centrifugal branch.

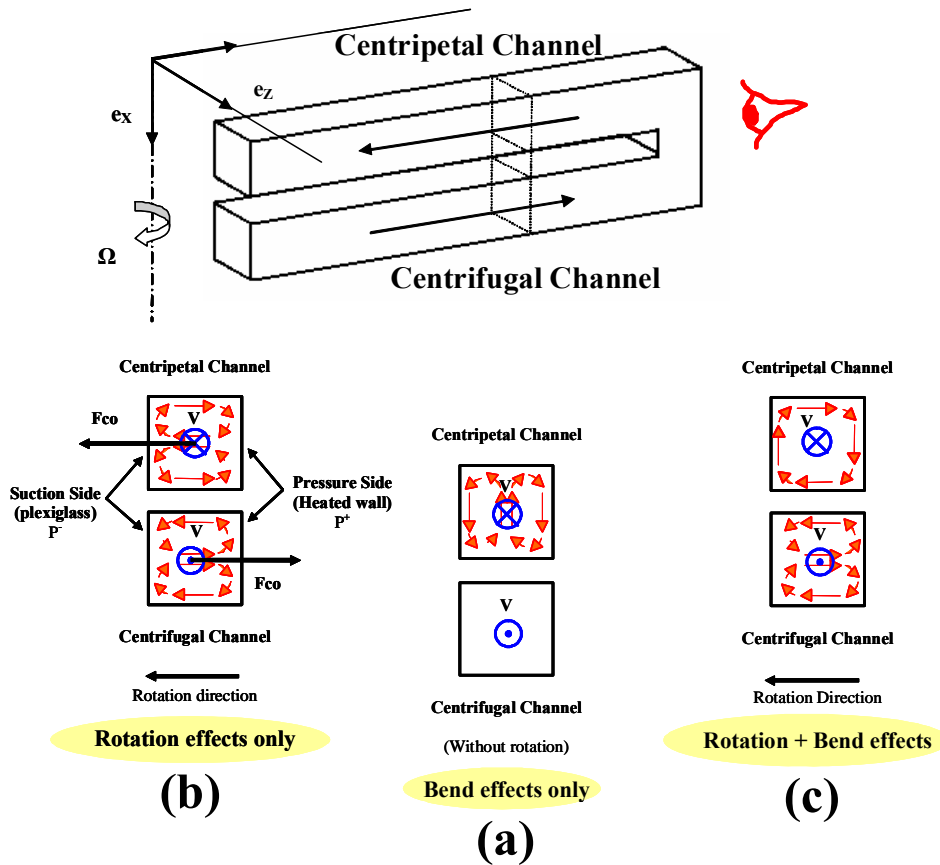


Figure 6: Secondary flows caused by rotation and bend.

5. Experimental Results and Discussion

5.1 Static case without ribs (heated wall: $T_w=333$ K)

Results presented (**Figure 7**) were obtained at a distance of $Z=20$ mm from the stainless steel wall. One wall of the channel was heated and its surface temperature was 333 K. The time duration between two consecutive laser pulses was set to $15 \mu s$ in order to meet the following requirements: large measurable velocity range (minimum/ maximum displacement of particle images) and spatial resolution of around 1 mm.

The average 3D-velocity field was reconstructed from 126 measurement planes (**Figure 7**). Due to the large model dimensions, six vertical planes (X direction) were needed for each section (Z direction) investigated. Turbulent flow in the centripetal channel with vortex formation downstream from the bend was evidenced.

The average velocities measured range from 0.4 m/s to 18.5 m/s in the present case (**Figure 7**).

The flow is accelerated at the outlet of the outward branch just upstream from the inner part of the bend. When the flow negotiates the 180° -turn, a recirculation zone is created at the inlet of the inward branch, which results in local high-velocities of the flow in the outer wall region.

The reattachment point downstream from the bend for the centripetal channel was observed to appear at the radial location $X=695$ mm.

The effect of bend curvature on internal heat transfer is shown by the spatial evolution of the ratio Nu/Nu_0 (**Figure 8**), which follows the velocity field closely. In other words, the higher the velocity levels near the walls, the higher the heat transfer coefficients (**Figure 8**).

The dimensionless velocity U_x/U_{mean} represents the ratio of radial velocity U_x to the mean bulk flow velocity at the channel inlet U_{mean} , with $U_{mean} = Re \cdot \mu / \rho \cdot D_H = 7.55$ m/s ($Re=25,000$ and $D_H=50$ mm).

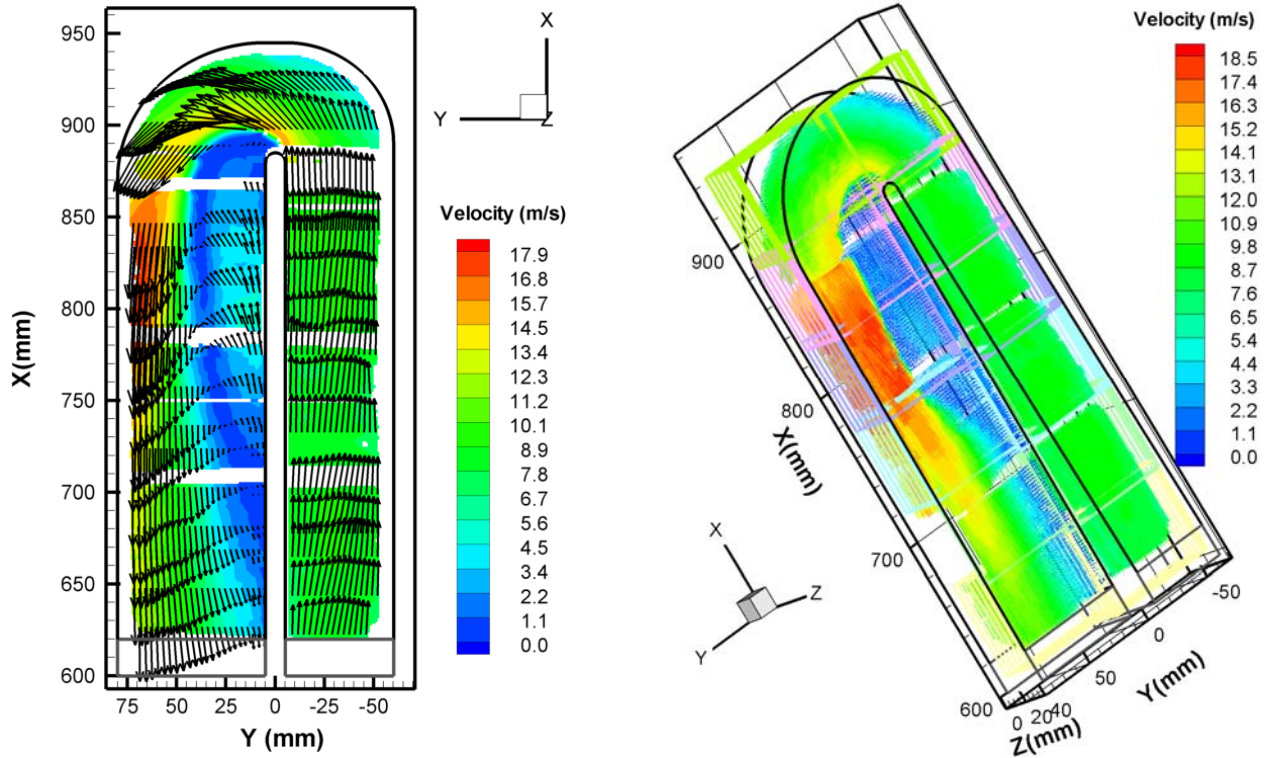


Figure 7: Velocity field results (left: $Z=20\text{mm}$ plane; right: 3D-field) obtained in the static case with heated wall ($Re=25,000$ $Ro=0$ $T_w=333$ K).

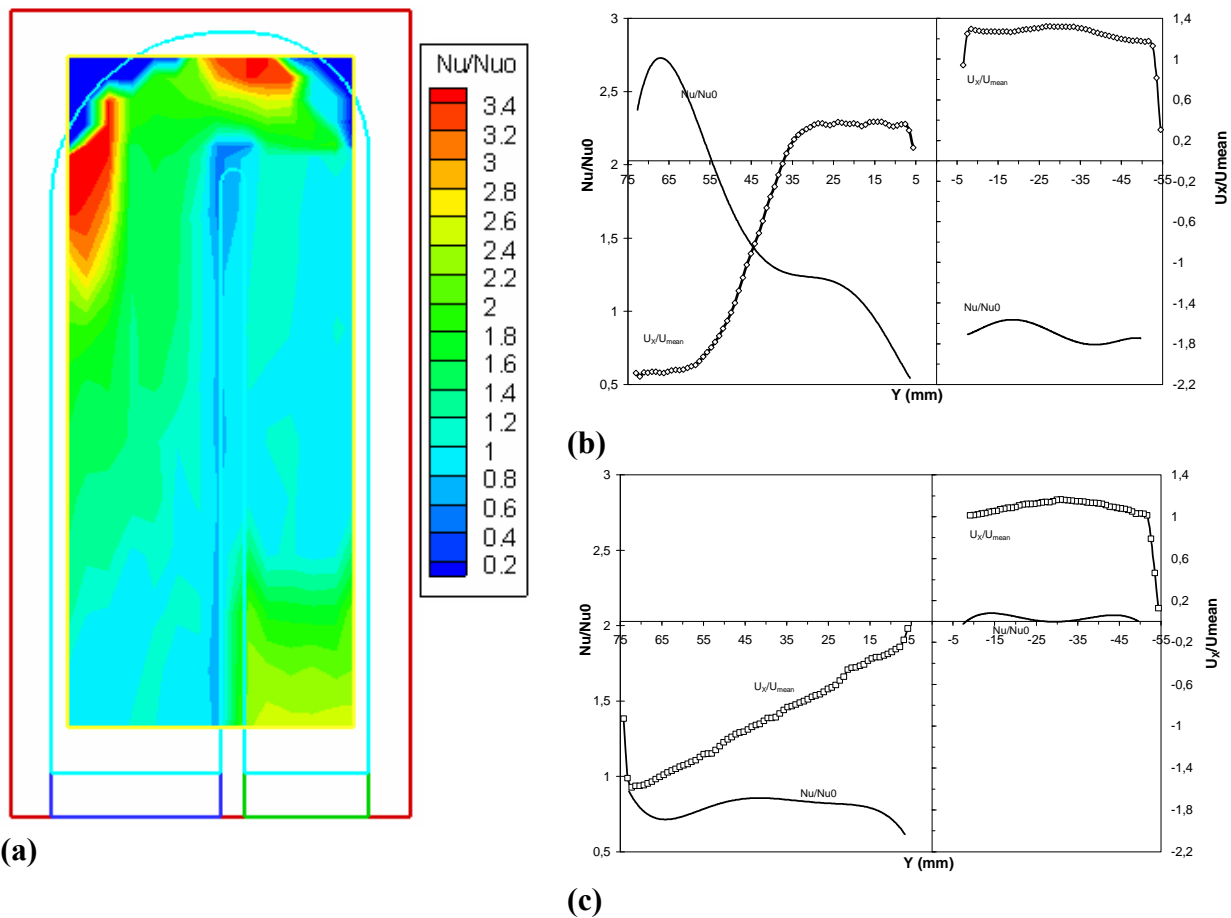


Figure 8: Nu/Nu_0 ratio (heat transfer coefficient) planar field results (a) deduced from thermal measurements over the stainless steel wall in the static case ($Re=25,000$ - $T_w=333$ K) - Normalized radial velocity (U_x/U_{mean}) and Nusselt (Nu/Nu_0) profiles at $X=850\text{mm}$ (b) and $X=650\text{mm}$ (c) in the static case ($Re=25,000$ - $Ro=0$ - $T_w=333$ K) for both branches of the channel (centripetal, left ; centrifugal, right).

5.2 Rotating case without ribs (heated wall: $T_w=333\text{ K}$)

Compared to the previous cases, the time duration between two consecutive laser pulses was reduced to $10\ \mu\text{s}$ in order to ensure a spatial overlap of the two regions illuminated by the laser sheets during rotation.

The average 3D-velocity field (**Figure 9**) was reconstructed from 73 measurement planes. Due to the large model dimensions, six vertical planes (X direction) were needed for each section (Z direction) investigated. The average velocities measured range from 0.4 m/s to 18.5 m/s in the present case.

The reattachment point downstream from the bend for the centripetal channel was observed to appear more rapidly in the rotating case ($X=813\text{ mm}$) compared to the static case ($X=695\text{ mm}$).

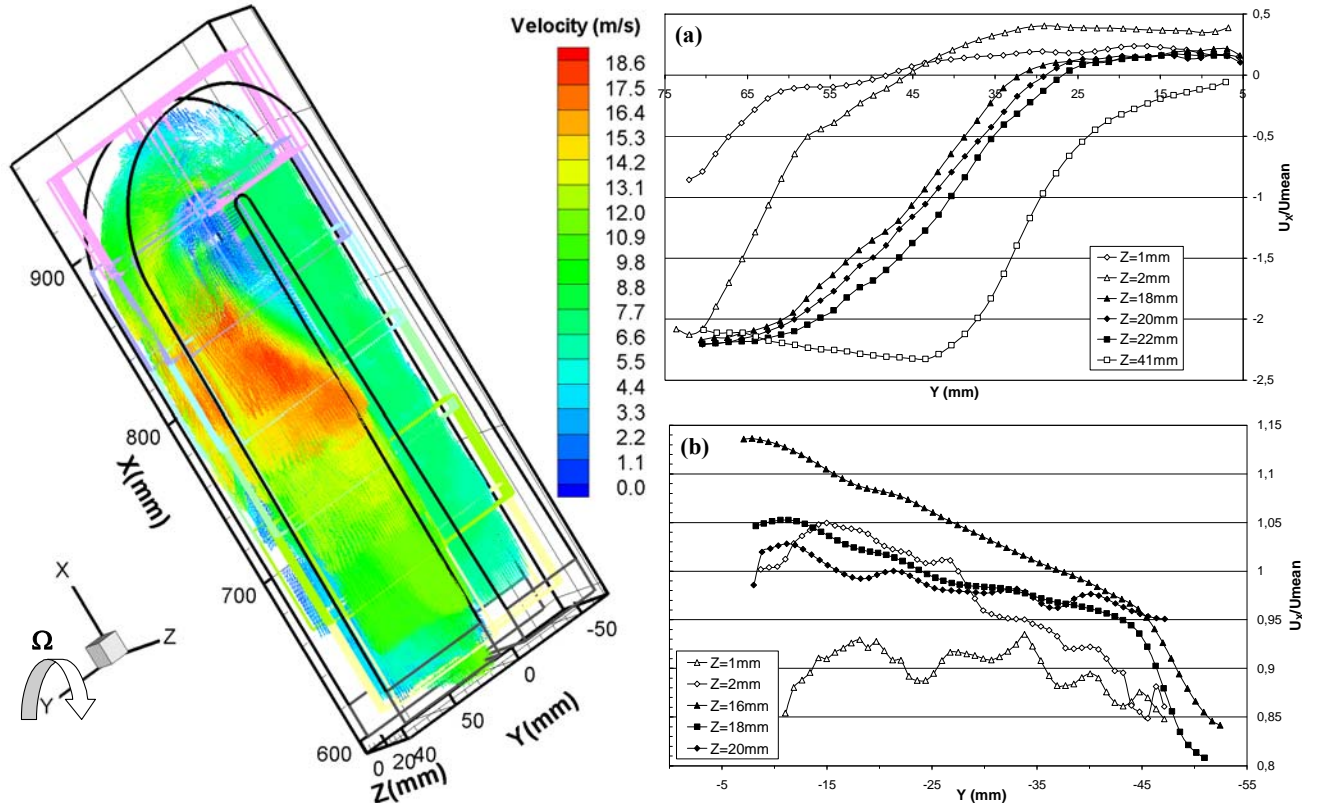


Figure 9: Velocity field results obtained in the rotating case with heated wall ($Re=25,000 - Ro=0.33 - T_w=333\text{ K}$), normalized radial velocity profiles (U_x/U_{mean}) at $X=850\text{ mm}$ for centripetal (a) and centrifugal (b) channels.

As shown in **Figure 6**, derived from previous studies [2], at the outlet of the bend (i.e. inlet of the centripetal branch), the secondary motion generated in the bend is coupled with the Coriolis-induced motion to create a single and large vortex exiting the bend; these two motions consist in two pairs of counter-rotating vortices shifted from each other by 90° .

In the centrifugal branch (**Figure 9-b** and **Figure 10-b**), the effect of rotation is identified the velocity vectors deflected toward the pressure side (stainless steel wall in present case).

Near the outlet of the bend, for $X=850\text{ mm}$, in the inlet part of the inward branch, a mean radial velocity as high as 2.3 times inlet mean radial velocity is observed in **Figure 9-a**.

In the centripetal branch (**Figure 9-a** and **Figure 10-a**), the effect of rotation is identified by velocity vectors deflected toward the suction side (plexiglass wall in present case).

A large secondary motion effect (single and large vortex exiting the bend) is identified downstream from the bend in the centripetal channel.

More downstream, for $X=650\text{ mm}$, not far from the outlet of the inward branch, the intensity of the single vortex decreases, with as a consequence lower variations of mean velocity profiles observed in Z direction (**Figure 10-a**).

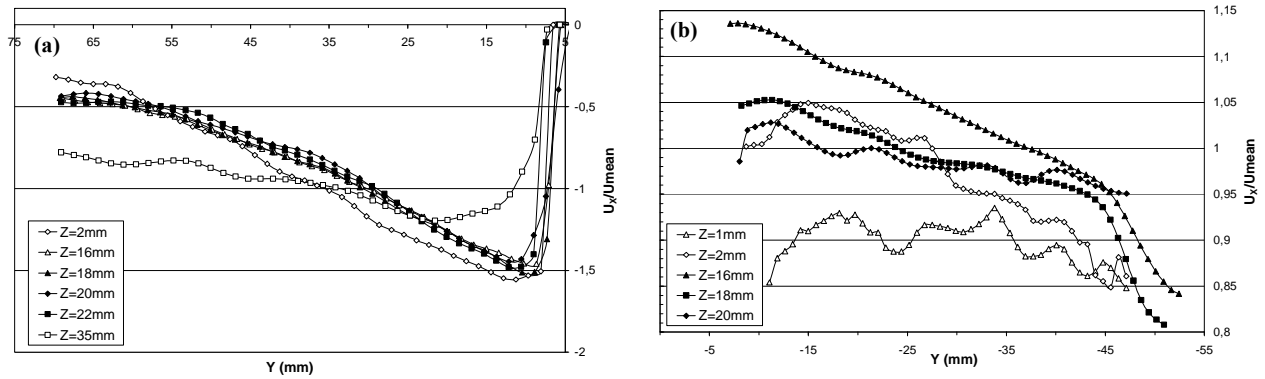


Figure 10: Radial velocity profiles (U_x/U_{mean}) at $X=650\text{mm}$ in the rotating case ($Re=25,000 - Ro=0.33 - T_w=333\text{K}$) for both branches of the channel: (a) centripetal; (b) centrifugal.

As observed in the static case, the flow is accelerated at the outlet of the outward branch just upstream the inner part of the bend.

This increase of local mean velocity is consistent with the increase of heat transfer coefficient measured by using the infrared camera (Figure 11).

The effect of motions induced by bend curvature and Coriolis forces on internal heat transfer are shown by the spatial evolution of the ratio Nu/Nu_0 (Figure 11), which follows the velocity field closely. As observed in the static case, the higher the velocity levels near the walls, the higher the heat transfer coefficients (Figure 11).

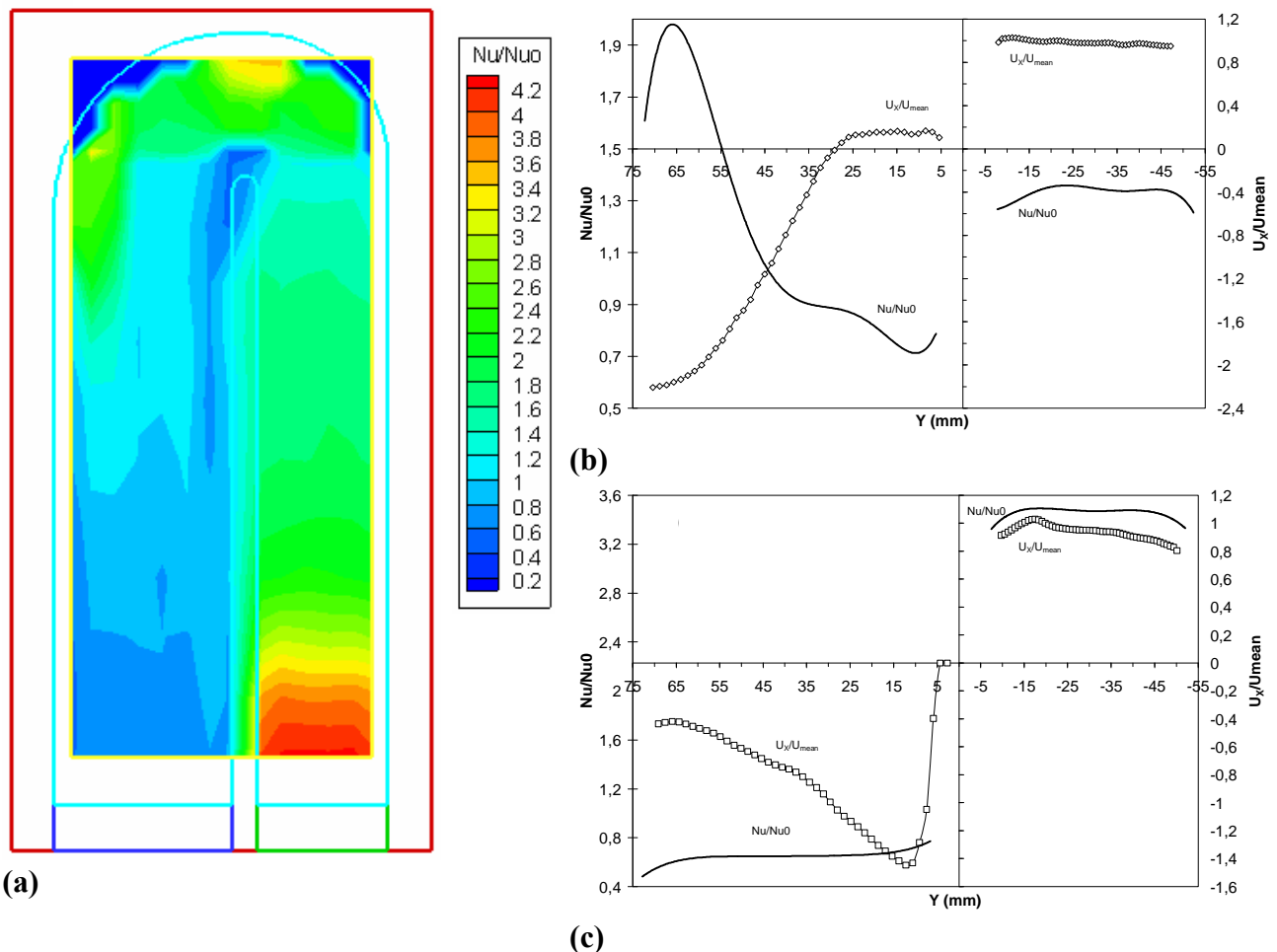


Figure 11: Nu/Nu_0 ratio (heat transfer coefficient) planar field results (a) deduced from thermal measurements over the stainless steel wall in the rotating case ($Re=25,000 - Ro=0.33 - T_w=333\text{ K}$) - Normalized radial velocity (U_x/U_{mean}) and Nusselt (Nu/Nu_0) profiles at $X=850\text{mm}$ (b) and $X=650\text{mm}$ (c) in the rotating case ($Re=25,000 - Ro=0,33 - T_w=333\text{ K}$) for both branches of the channel (centripetal, left ; centrifugal, right).

5.3 Static and rotating cases with ribs (heated wall: $T_w=333\text{ K}$)

The U-bend test section reproducing a part of a cooling passage is now equipped with 16 ribs disposed on the heated wall (**Figure 12**). Ribs are inclined at 45° , cross-section ribs is $5\text{ mm} \times 5\text{ mm}$ with a regular interval of 37.5 mm between every rib.

Results presented for the Ribbed Channel were obtained for same operating conditions and analyzed also in comparison with Smooth Channel previous results [1] in static and rotating cases.

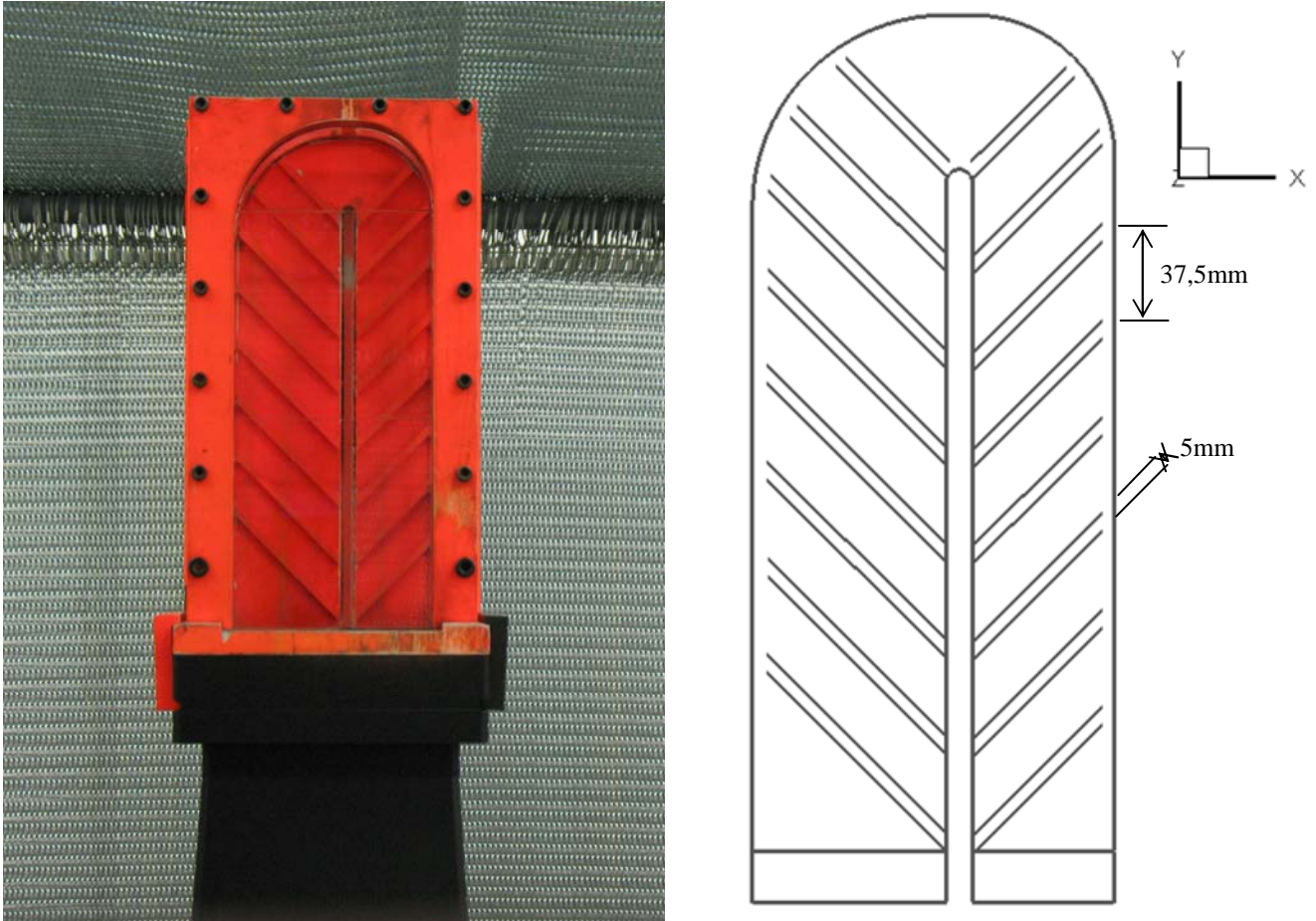


Figure 12: Photographs of the test channel (ribbed configuration) and position of ribs.

The influence of ribs on the flow structure in the bend and in the centripetal channel is evidenced in **Figure 13** without rotation and in **Figure 14** with rotation.

In both cases, the flow is accelerated at the outlet of the outward branch just upstream from the inner part of the bend. When the flow negotiates the 180° -turn, a recirculation zone is created at the inlet of the inward branch, which results in local high-velocities of the flow in the outer wall region.

For the smooth channel configuration, a close recirculation followed by a reattachment point downstream from the bend for the centripetal channel was observed.

For the ribbed channel configuration, an open recirculation zone is observed downstream from the bend.

In both cases (smooth or ribbed walls channels), the length of recirculation zones was reduced by the effect of rotation.

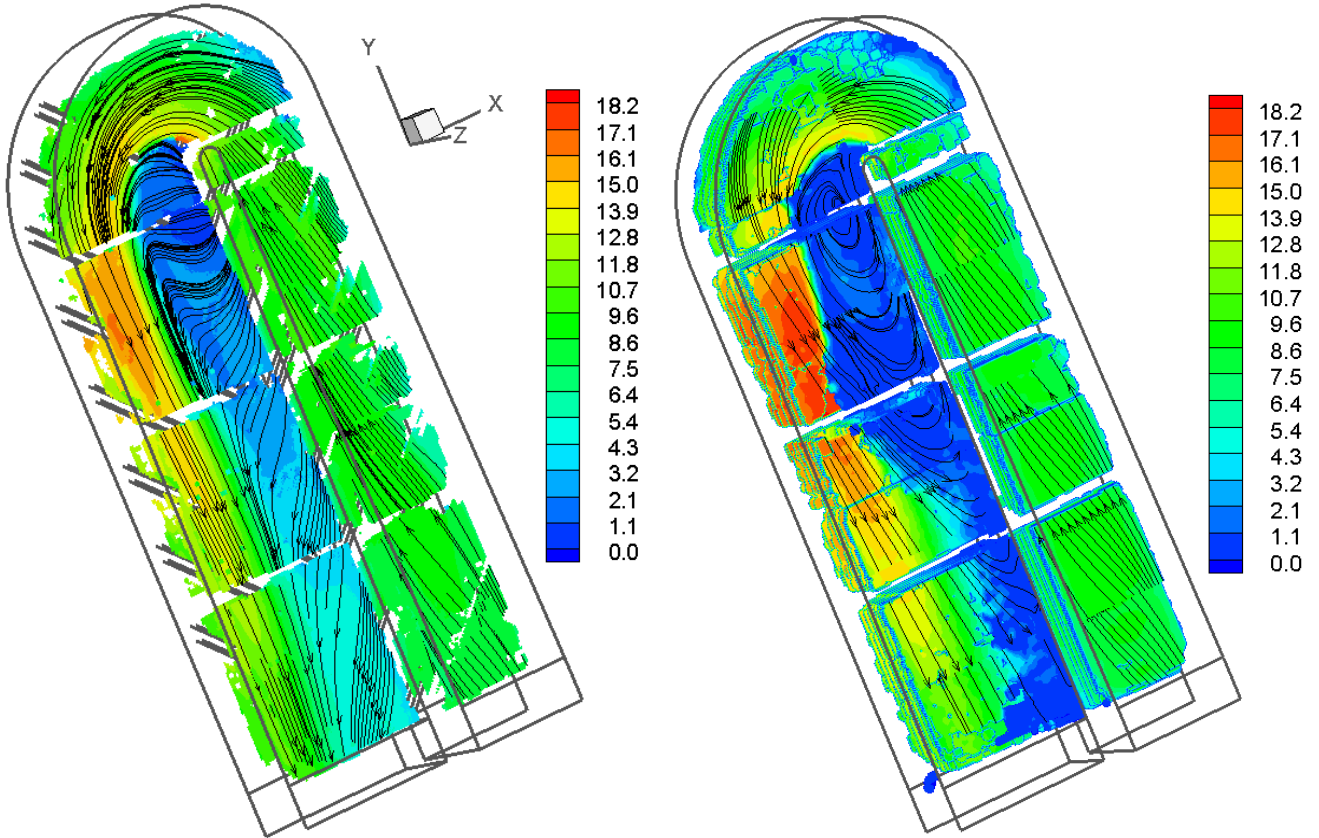


Figure 13: Velocity magnitude and streamtraces obtained in the static case ($Re=25\ 000$, $Ro=0$, $T_w=333\ K$) for the ribbed channel (left) compared to the smooth channel (right).

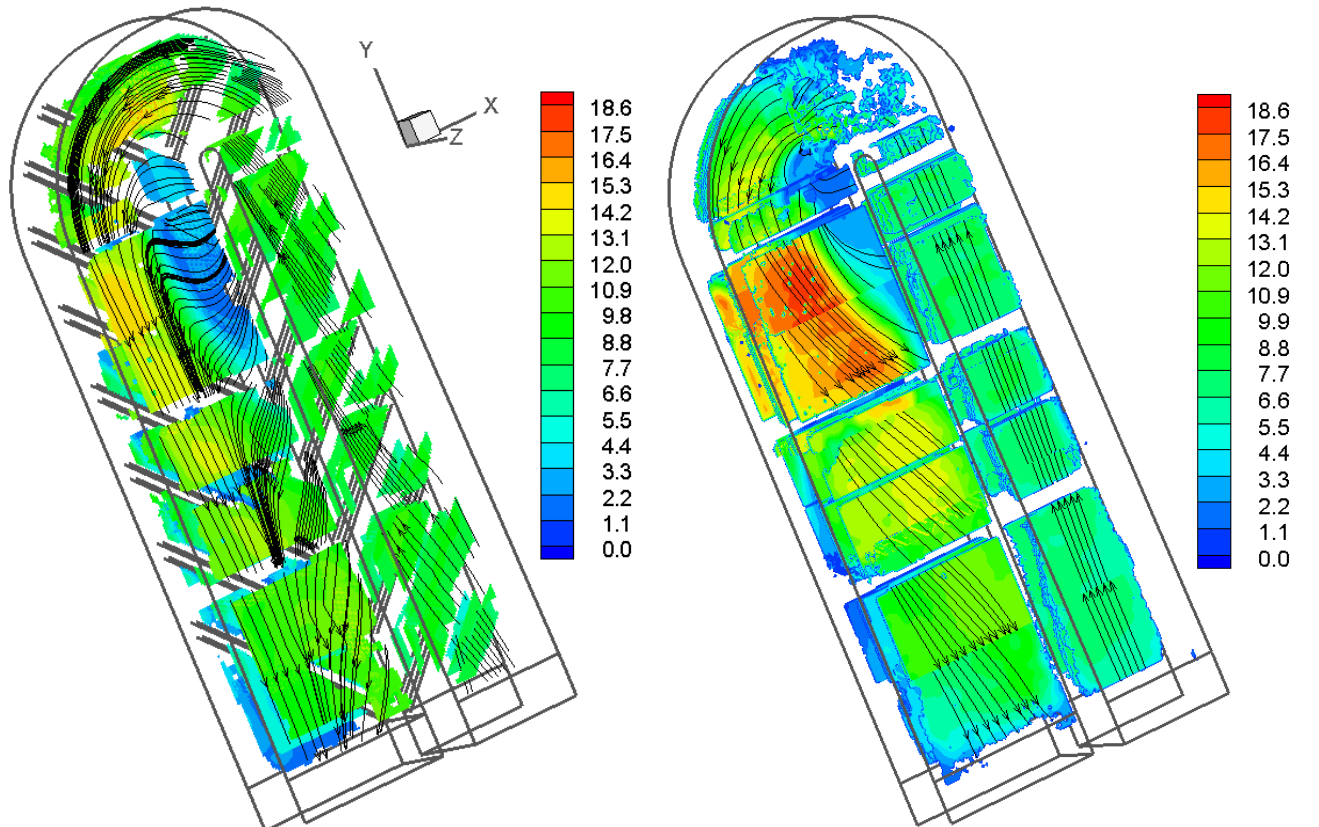


Figure 14: Velocity magnitude and streamtraces obtained in the rotating case ($Re=25\ 000$, $Ro=0.33$, $T_w=333\ K$) for the ribbed channel (left) compared to the smooth channel (right).

6. Computational results and comparison with experimental results

CEDRE® is the code used for mainly energetics applications at ONERA. Its main application domain concerns internal flows in aerospace engines [5]. Experimental results have been confronted with computational results for the smooth channel and have been useful to choose turbulence and wall laws models adapted to those types of flows.

6.1 Computation strategy used: CEDRE® CFD code

CEDRE® is a solver platform developed by ONERA and designed for industrial purposes [6] [7]; it runs computations on unstructured meshes and its solver named CHARME has been used: it is a 3D Navier-Stokes solver, using an second order upwind Roe scheme in space (MUSCL reconstruction and Van Leer Limiters techniques) and an implicit scheme for time integration. Present calculations used the EARSM (Explicit Algebraic Reynolds Stress Model of Wallin and Johansson) turbulence model for its ability to simulate rotating flows [4]. For same purpose, ONERA has developed an advanced wall function named SIBLE (Simple Integrated Boundary Layer Equations) [8], able to take into account pressure gradients. This wall model locally solves a set of boundary layer equations and provides a good evaluation of the friction and heat exchange coefficients, compared to conventional wall functions. The objective of these calculations is the validation of these two models in a representative configuration of turbine blade cooling passages.

The computational domain has been meshed using CENTAUR in a 3D unstructured grid; only 690 000 cells are used to discretize the whole domain. As shown in **Figure 15**, the inlet circuit is quite complex, due to the junction between the primary circuit on the rotating axis and the centrifugal channel, which induces a swirl (**Figure 16**). It is essential to reproduce this upstream condition in order to accurately simulate the flow and compare the results to the measurements.

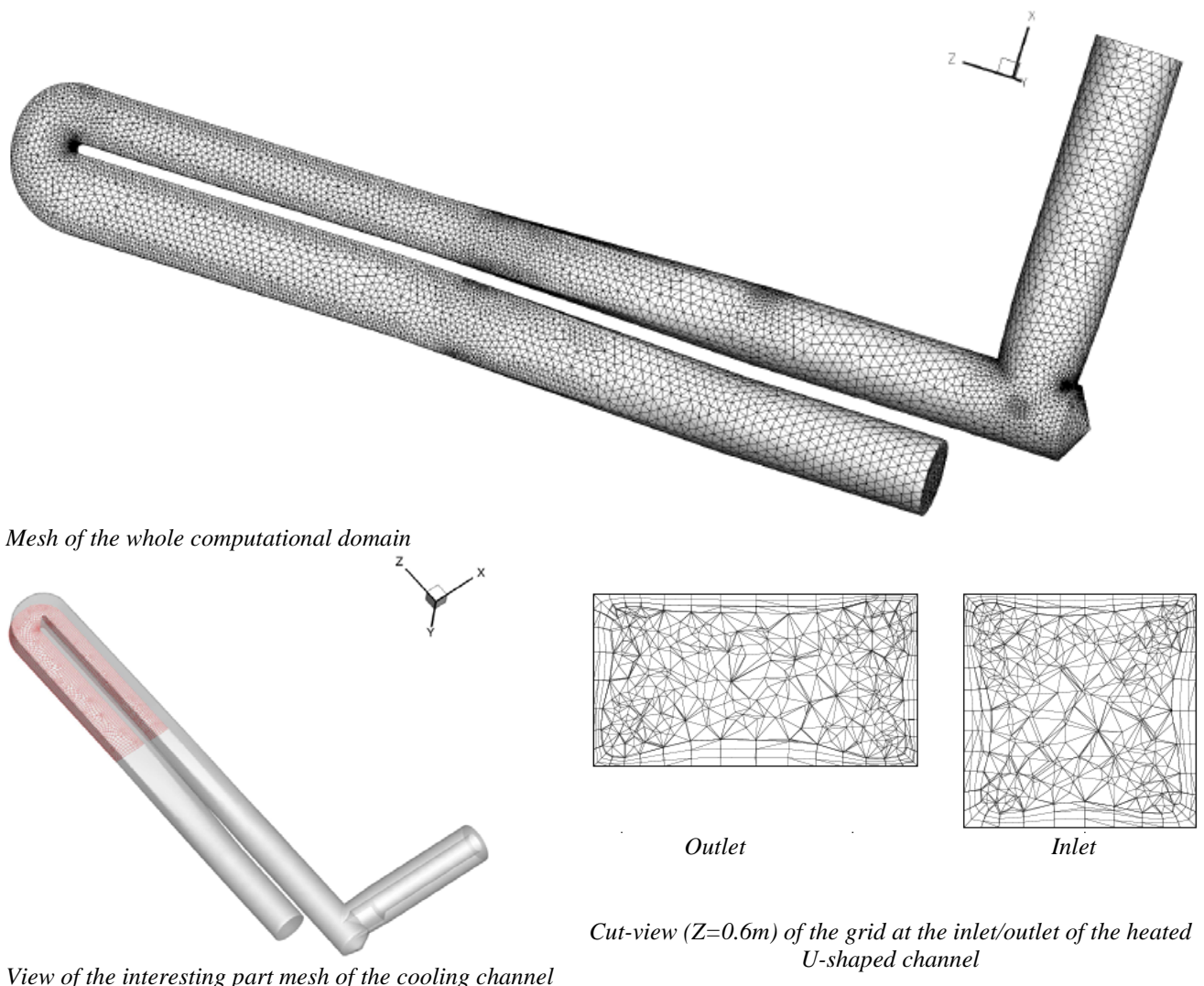


Figure 15: Global view of the computational domain and coarse mesh

6.1 Numerical simulations of the static case (Re=25 000)

Comparisons between PIV measurements and computational results (**Figure 16**) show that the flow is well reproduced by the CEDRE code, using the retained models described above. **Figure 17** illustrates, for the static case, this good agreement: on both two planes considered, corresponding to distances from the heated wall of 20mm and 25mm, we could clearly identify two separation zones, placed identically in both the simulation and the measurements.

This simulation realized with EARSM turbulence and SIBLE wall law models allows a quite good description of the flow on a coarse mesh, especially in rotation. Comparisons of experimental results with k- ω turbulence model associated with standard analytic wall law were not so good, in particular in rotation mode. It proved the EARSM is handling way better the rotational effects.

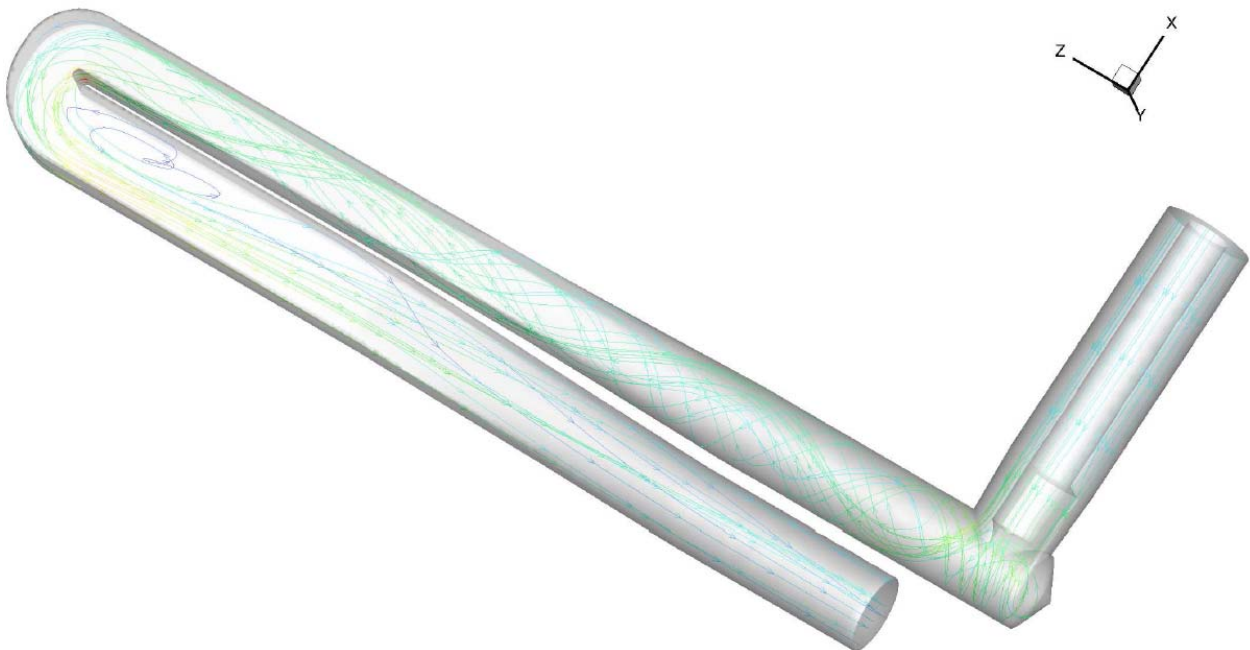


Figure 16: Streamtraces calculated in static configuration (Re=25 000)

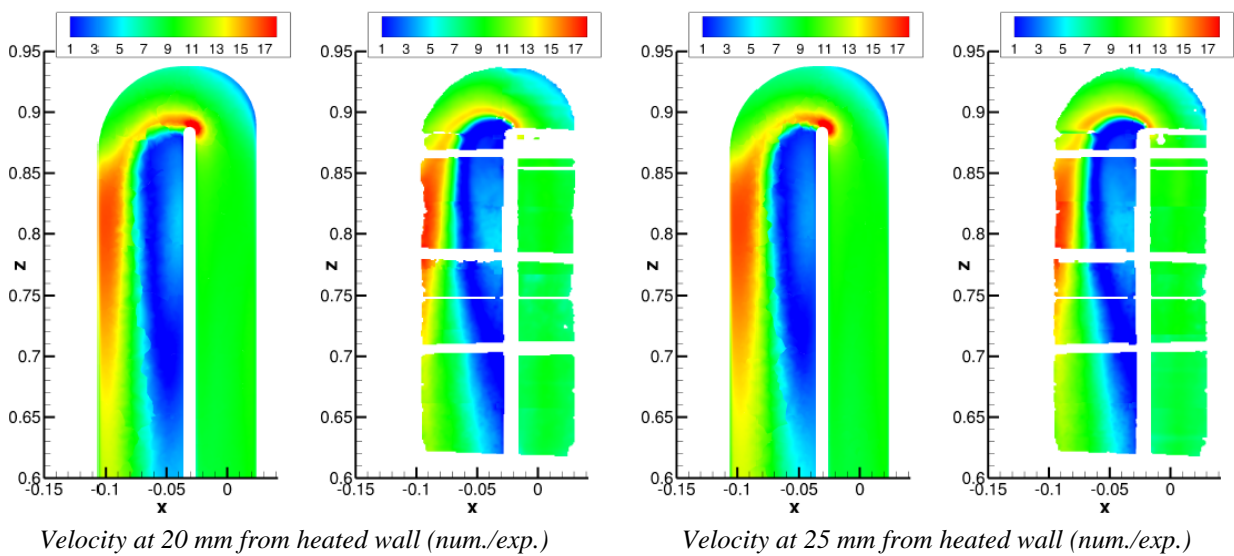


Figure 17: Comparison between computation and experiment of the velocity magnitude for two positions (Ro=0).

6.2 Numerical simulations of the rotating case ($Re=25\ 000$, $Ro=0.33$)

Results in the rotating case show that the reduction of the recirculation zone (**Figure 18**) is well captured by the CEDRE code. **Figure 19** illustrates, for the rotating case, this good agreement, even if a velocity deficit is observed from the inlet plane of the U-bend duct until the exit plane. This deficit may be attributed to a bad description of the inlet swirl by the coarse grid mentioned earlier. However, on both two planes considered (**Figure 19**), corresponding to distances from the heated wall of 18mm and 22mm, we could clearly identify zones, located at the same place in both the simulation and the measurements.



Figure 18: Streamtraces calculated in rotating configuration ($Re=25\ 000$, $Ro=0.33$)

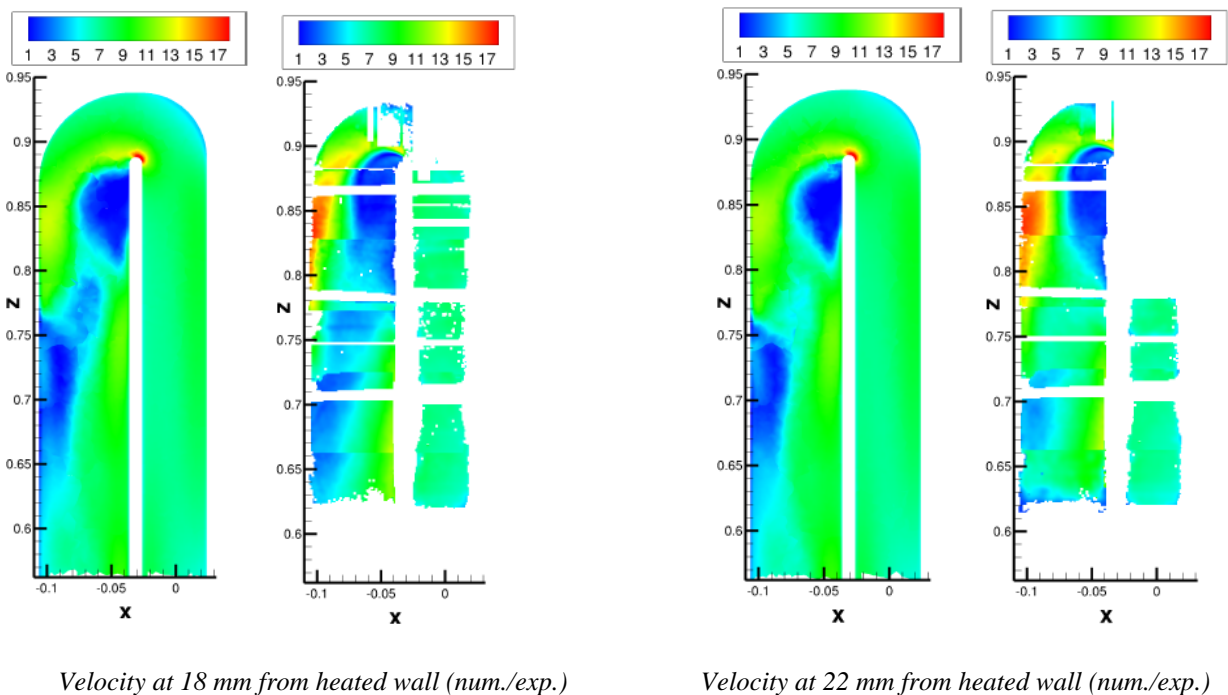


Figure 19: Comparison between computation and experiment of the velocity magnitude for two positions ($Ro=0.33$).

7. Conclusions

The knowledge of flow and heat transfer characteristics inside internal cooling channels is required to optimize the geometry while increasing thermal efficiency. The BATHIRE large-scale test rig has been designed and tested in order to set up an experimental database for non-rotating and rotating flow cases. Experimental results obtained by using the Particle Image Velocimetry (P.I.V.) and Infrared thermography techniques in this new facility named BATHIRE (Test Bench for AeroThermal flows Investigations in a Rotating Environment) were described in this paper. PIV measurements were performed in the centrifugal and centripetal branches of smooth and ribbed channels. The use of the PIV technique (for flow fields measurements) associated with Infrared thermometry (for thermal measurements) has provided a useful database for validation of CFD codes.

Detailed conclusions issued from this experimental study are the followings:

- For each experimental case investigated, the averaged velocity field was reconstructed from more than 70 measurement planes (this work was consequently very time consuming for the management of experiments as well as for the data processing).
- In the centrifugal branch, the effect of rotation is identified by velocity vectors deflected toward the pressure side.
- In the centripetal branch, the effect of rotation is identified by velocity vectors deflected toward the suction side.
- For the smooth channel case, a close recirculation followed by a reattachment point downstream from the bend for the centripetal channel was observed. For the ribbed channel configuration, an open recirculation zone is observed.
- At the outlet of the bend and at the inlet of the centripetal branch, the secondary motion generated in the bend is coupled with the Coriolis-induced motion to create a single and large vortex exiting the bend plane.
- The reattachment point downstream from the bend for the centripetal channel was observed to appear more rapidly in the rotating case ($X=813\text{mm}$) compared to the static case ($X=695\text{mm}$) for the smooth channel. Same phenomena are observed for the length of the open recirculation observed for the ribbed channel.
- The increase of local mean velocity is mainly consistent with the increase of heat transfer coefficient measured by using an infrared camera.

Other experimental conditions tested and not presented in this paper, such as a reverse direction of rotation ($\Omega < 0$) are also available in the database in order to complete the CFD validation.

The goal of these experimental studies is mainly the validation of numerical codes. Validation of flow physical models needs to be applied on elementary through representative configurations before its use for the flow and heat transfer evaluations inside various and complex cavities. Simulations realized with EARSM turbulence and SIBLE wall law models allow a quite good description of the flow on a coarse mesh, especially in rotation. Comparisons of experimental results with $k-\omega$ turbulence model associated with standard analytic wall law were not so good, in particular in rotation mode. It proved the EARSM is handling way better the rotational effects.

The use of the PIV technique (for flow fields measurements) associated with Infrared thermometry (for thermal measurements) on simplified models mounted to BATHIRE facility should allow providing useful databases for evaluation and validation of CFD codes.

References

- [1] A. Ristori, Y. Servouze, M. Barat, F. Soullignac. 2007. P.I.V. Flow Characterization Inside a Large-Scale U-Shaped Rotating Channel, 7th International Symposium on Particle Image Velocimetry. *PIV 2007, Roma, Italy, September 11-14, 2007*.
- [2] C. Brossard, Y. Servouze, P. Gicquel, R. Barrier. 2005. Characterization of the flow field inside a rotating, rib-roughened, U-shaped channel using particle image velocimetry. *International congress on instrumentation in aerospace simulation facilities, Sendai (Japan), August 29 – September 2, 2005*.
- [3] A. Ristori, Y. Servouze, M.P. Errera, D. Dutoya, J. Perruchini. 1991. Numerical simulation of flows inside internal cavities of turbine rotor blade. *Eurotherm seminar n° 25 "Heat transfer in single phase flows", Pau (France), July 8-9, 1991*.
- [4] F. Guillou, F. Chedevergne. 2011. Internal turbine blade cooling simulation: advanced models assessment on ribbed configurations. *Proceedings of the ASME/JSME 2011 8th Thermal Engineering Joint Conference, AJTEC2011, March 13-17, 2011, Honolulu, Hawaii, USA*.
- [5] D. Scherrer and al. 2011. Recent CEDRE Applications, CFD Platforms and Coupling - *Journal AerospaceLab, the ONERA Journal – Issue 2- March 2011* - <http://www.aerospacelab-journal.org/>.
- [6] P. Chevalier and al. 2005. Cedre: Development and validation of a multiphysic computational software – *Eucass Proceedings of the EUCASS 2005 European Conference for Aero-Space Sciences, 7 July 2005, Moscow, Russia*.
- [7] CEDRE® Website: <http://cedre.onera.fr>
- [8] F. Chedevergne. 2010. Advanced Wall Model for Aerothermodynamics. *International Journal of Heat and Fluid Flows, Volume 31, Issue 5, October 2010, Pages 916–924*